AMERICAN SOCIETY FOR MICROBIOLOGY | Applied and Environmental Microbiology®

BIOTECHNOLOGY

Increasing the Thermodynamic Driving Force of the Phosphofructokinase Reaction in *Clostridium thermocellum*

Shuen Hon,[a,b,c] Tyler Jacobson,[b,d] David M. Stevenson,[b,d] Marybeth I. Maloney,[a,b] Richard J. Giannone,[b,e] Robert L. Hettich,[b,e] Daniel Amador-Noguez,[b,d] Daniel G. Olson,[a,b] Lee R. Lynd[a,b,c]

[a]Thayer School of Engineering, Dartmouth College, Hanover, New Hampshire, USA
[b]Center for Bioenergy Innovation, Oak Ridge, Tennessee, USA
[c]Enchi Corporation, Hanover, New Hampshire, USA
[d]Department of Bacteriology, University of Wisconsin—Madison, Madison, Wisconsin, USA
[e]Biosciences Division, Oak Ridge National Laboratory, Oak Ridge, Tennessee, USA

ABSTRACT Glycolysis is an ancient, widespread, and highly conserved metabolic pathway that converts glucose into pyruvate. In the canonical pathway, the phosphofructokinase (PFK) reaction plays an important role in controlling flux through the pathway. *Clostridium thermocellum* has an atypical glycolysis and uses pyrophosphate (PP_i) instead of ATP as the phosphate donor for the PFK reaction. The reduced thermodynamic driving force of the PP_i-PFK reaction shifts the entire pathway closer to thermodynamic equilibrium, which has been predicted to limit product titers. Here, we replace the PP_i-PFK reaction with an ATP-PFK reaction. We demonstrate that the local changes are consistent with thermodynamic predictions: the ratio of fructose 1,6-bisphosphate to fructose-6-phosphate increases, and the reverse flux through the reaction (determined by ^{13}C labeling) decreases. The final titer and distribution of fermentation products, however, do not change, demonstrating that the thermodynamic constraints of the PP_i-PFK reaction are not the sole factor limiting product titer.

IMPORTANCE The ability to control the distribution of thermodynamic driving force throughout a metabolic pathway is likely to be an important tool for metabolic engineering. The phosphofructokinase reaction is a key enzyme in Embden-Mayerhof-Parnas glycolysis and therefore improving the thermodynamic driving force of this reaction in *C. thermocellum* is believed to enable higher product titers. Here, we demonstrate switching from pyrophosphate to ATP does in fact increases the thermodynamic driving force of the phosphofructokinase reaction *in vivo*. This study also identifies and overcomes a physiological hurdle toward expressing an ATP-dependent phosphofructokinase in an organism that utilizes an atypical glycolytic pathway. As such, the method described here to enable expression of ATP-dependent phosphofructokinase in an organism with an atypical glycolytic pathway will be informative toward engineering the glycolytic pathways of other industrial organism candidates with atypical glycolytic pathways.

KEYWORDS *Clostridium*, metabolomics, metabolic engineering, advanced biofuels, *Clostridium thermocellum*

Clostridium thermocellum is a promising candidate for production of lignocellulosic biofuels due to its strong native ability to consume cellulose. Metabolic engineering has resulted in strains that produce ethanol at high yield (>80% of theoretical) (1–3). However, titers above 30 g/L have not been achieved (1, 2, 4), thus limiting commercial viability of the engineered strains (5).

C. thermocellum belongs to a group of organisms that specialize in cellulose fermentation. These organisms typically have a limited substrate range, preferring to grow on crystalline cellulose and its hydrolysis products (6). For many of them, Embden-Mayerhof-Parnas

Editor Haruyuki Atomi, Kyoto University

Address correspondence to Daniel G. Olson, daniel.g.olson@dartmouth.edu.
The authors declare a conflict of interest. Lee R. Lynd and Shuen Hon are affiliated with Enchi Corporation, which has a financial interest in engineering *Clostridium thermocellum*.

Received 26 July 2022
Accepted 10 September 2022
Published 26 October 2022

(EMP) glycolysis is the only pathway for substrate assimilation, although several variations are present (7). In these organisms, glycolysis appears to be closer to thermodynamic equilibrium (8, 9), in part due to the different cofactor usage for several of its reactions (8). In the case of *C. thermocellum* glycolysis, it was previously found that pyrophosphate (PP_i) was the main cofactor used in the 6-phosphofructokinase (PFK) reaction instead of ATP; in addition PP_i is also necessary for conversion of phosphoenolpyruvate to pyruvate via the pyruvate-phosphate dikinase (PPDK) reaction. It was also previously demonstrated that biosynthetic reactions were insufficient to account for the PP_i needed to explain glycolytic flux, suggesting therefore that a nonbiosynthetic reaction was responsible for generating the majority of the PP_i needed by glycolysis (10). A recent study attempted to identify the primary source of PP_i, but the findings were inconclusive (11).

Among these several atypical aspects of *C. thermocellum* glycolysis (10), the use of PP_i instead of ATP as a high-energy phosphate donor for the PFK reaction has a large effect on the overall thermodynamics of the pathway for several reasons. One is that the standard Gibbs free energy of the PP_i-PFK reaction (EC 2.7.1.90, $\Delta_r G'^\circ = -4.6 \pm 1.4$ kJ/mol) is lower than that of the ATP-PFK reaction (EC 2.7.1.11, $\Delta_r G'^\circ = -17.8 \pm 1.3$ kJ/mol) (12). Another is that the ATP/ADP ratio is around 10 in many organisms, whereas the PP_i/P_i ratio is around 0.1 (13), which serves to increase the thermodynamic driving force of the ATP-linked reaction, while decreasing the driving force of the PP_i-linked reaction. The low thermodynamic driving force of the PP_i-PFK reaction can explain both the high reversibility of glycolysis in this organism and the large size of the intracellular hexose phosphate pools (glucose-6-phosphate [G6P] and fructose-6-phopshate [F6P]) in this organism compared to organisms with canonical glycolysis, such as *Escherichia coli* and *Thermoanaerobacterium saccharolyticum*, where the hexose phosphate pools are much smaller (8). It may also explain the low ethanol tolerance of *C. thermocellum*.

Growth *of C. thermocellum* is inhibited in the presence of 5 g/L ethanol and completely inhibited at concentrations of 15 g/L (14). A comparison of changes to relative intracellular metabolite concentrations in both *C. thermocellum* and *T. saccharolyticum* in the presence of increasing ethanol concentrations revealed that concentrations of glycolytic intermediates began to accumulate in *C. thermocellum* cells at much lower ethanol concentrations than in *T. saccharolyticum* (15). Of note, the relative concentrations of the hexose phosphate (G6P and F6P) pool—both being immediately upstream of the PFK reaction—increased significantly as a result of ethanol addition in *C. thermocellum*, whereas in *T. saccharolyticum* the relative hexose phosphate pool sizes remained relatively similar between the control and ethanol addition experiments, indicating that in *C. thermocellum*, this reaction is close to thermodynamic equilibrium and the upstream metabolite pool sizes are largely controlled by mass action effects.

The free energy change of a reaction can also be determined by measuring the relative forward and reverse flux in a reaction (16). In brief, a more thermodynamically favorable reaction will exhibit greater forward flux than reverse flux. Isotope labeling experiments where cells are fed a mixture of naturally labeled and universally labeled substrates can be used to determine the relative forward and reverse fluxes of a reaction, allowing one to infer differences in free energy changes (16, 17). Experiments with ^{13}C-labeled substrates have shown that glycolysis is much closer to thermodynamic equilibrium in *C. thermocellum* compared to organisms that use the canonical pathway (e.g., *E. coli* and *T. saccharolyticum*) (8).

Furthermore, a thermodynamic analysis of elementary flux modes of alternative glycolytic pathways identified the PP_i-PFK reaction as one of three important genetic interventions for increasing the overall thermodynamic driving force of the cellobiose to ethanol pathway (18).

Finally, in experiments designed to increase product titer by growing *C. thermocellum* in the presence of high concentration of substrate, a significant fraction of the substrate is left unconsumed or converted to products upstream of glycolysis (i.e., glucose) (1, 4).

These converging lines of evidence are the basis for our hypothesis that the low thermodynamic driving force of the PP_i-PFK reaction limits ethanol titer in *C. thermocellum* and

TABLE 1 Strains used in this study

Strain	Organism	Description	Accession no.	Source or reference(s)
LL1004	*C. thermocellum*	DSM 1313	CP002416	DSMZ
LL1025	*T. saccharolyticum*	Strain JW/YS-485L	CP003184	42
LL1570	*C. thermocellum*	Engineered *C. thermocellum* with *T. saccharolyticum* pyruvate to ethanol pathway (*T. saccharolyticum adhA*, *nfnAB*, *adhE*^{G544D}, *pforA*, ferredoxin), deletion of *C. thermocellum pfors*	SRP144049	1, 23
LL1592	*C. thermocellum*	LL1570 Δ*ldh*	SRP181986	This study
L1647	*C. thermocellum*	LL1592 *PP$_i$-pfk*::*pTsac_0327-Tsac_0327*	SRP222666	This study
LL1648	*C. thermocellum*	LL1647 *Clo1313_0718*::*Tsac_1362*	SRP222662	This study
LL1649	*C. thermocellum*	LL1648 Δ*Clo1313-0717-0718*::*pTsac_1362*	SRP222669	This study
LL1660	*C. thermocellum*	LL1649 Δ*Clo1313_1876* Δ*tal*	SRP246483	This study
LL1661	*C. thermocellum*	Sister colony #1 of LL1660	SRP246561	This study
LL1662	*C. thermocellum*	Sister colony #2 of LL1660	SRP246510	This study
LL1663	*C. thermocellum*	Sister colony #3 of LL1660	SRP246511	This study
T7 express	*E. coli*	*fhuA2 lacZ*::*T7 gene1 [lon] ompT gal sulA11 R*(*mcr-73*::*miniTn10–TetS*)*2 [dcm] R*(*zgb-210*::*Tn10–TetS*) *endA1* Δ(*mcrC-mrr*)*114*::*IS10*		NEB[a]

[a]New England Biolabs, Ipswich, MA.

that replacing that enzyme with an ATP-linked enzyme would increase ethanol titer by allowing for more complete substrate consumption and reducing inhibition by product accumulation. It should be noted that the *C. thermocellum* genome contains a putative ATP-*pfk* gene, *Clo1313_0997* (19); however, enzymatic assays to determine the cofactor usage of the PFK reaction in *C. thermocellum* indicate that the reaction is exclusively PP_i dependent, with no detectable ATP-dependent activity (10), suggesting that either this native ATP-Pfk was inactive or possessing activity below our limit of detection in cell extracts, or that our assay conditions were not suitable for measuring its activity. Due to this observation, and that the native ATP-Pfk is not fully characterized and understood, it was decided that expressing a heterologous ATP-*pfk*—in this study taken from *T. saccharolyticum* (20)—with detectable activity was necessary.

One factor that complicates a simple replacement of PP_i-*pfk* with ATP-*pfk* in *C. thermocellum* is that the PP_i-dependent phosphofructokinase enzyme in *C. thermocellum* is believed to have an additional role in the nonoxidative pentose phosphate pathway, where it catalyzes the interconversion of sedoheptulose-7-phosphate (S7P) to sedoheptulose-1,7-bisphosphate (SBP) (19, 21, 22) to allow for interconversion of hexoses and pentoses. Deleting the PP_i-Pfk protein from *C. thermocellum* would therefore disrupt not only glycolysis but also the pentose phosphate pathway. In the direction of hexose to pentose conversion, SBP must be converted to S7P (21, 22). The high thermodynamic driving force of the ATP-Pfk enzyme effectively prevents the reverse reaction, and it therefore appears necessary to introduce transaldolase activity to allow replacement of the PP_i-*pfk* gene with and ATP-*pfk* gene.

In this study, we investigated the effect of changing the phosphate donor of the PFK reaction from PP_i to ATP on the thermodynamic driving force of glycolysis in *C. thermocellum* by deleting the native *PP$_i$-pfk* gene (*Clo1313_1876*) and expressing a heterologous *ATP-pfk* gene from *T. saccharolyticum* (*Tsac_1362*).

RESULTS

Decoupling glycolysis from the pentose phosphate pathway. Strain LL1570 (1) (Table 1) was chosen as the reference strain for this study since it incorporates previous engineering with the *T. saccharolyticum* pyruvate to ethanol pathway—expression of *T. saccharolyticum adhA*, *nfnAB*, *adhE*^{G544D}, *pforA*, and ferredoxin (1, 23)—to improve ethanol yield and titer; this made it the logical starting point for metabolic engineering efforts to further improve ethanol titer. In addition, since lactate is a minor but nonetheless undesired byproduct of *C. thermocellum* fermentation (24), the *ldh* gene was deleted from strain LL1570 to create strain LL1592 to redirect carbon flux from lactate to ethanol production. Following the *ldh* deletion, the first step in replacing PP_i-linked

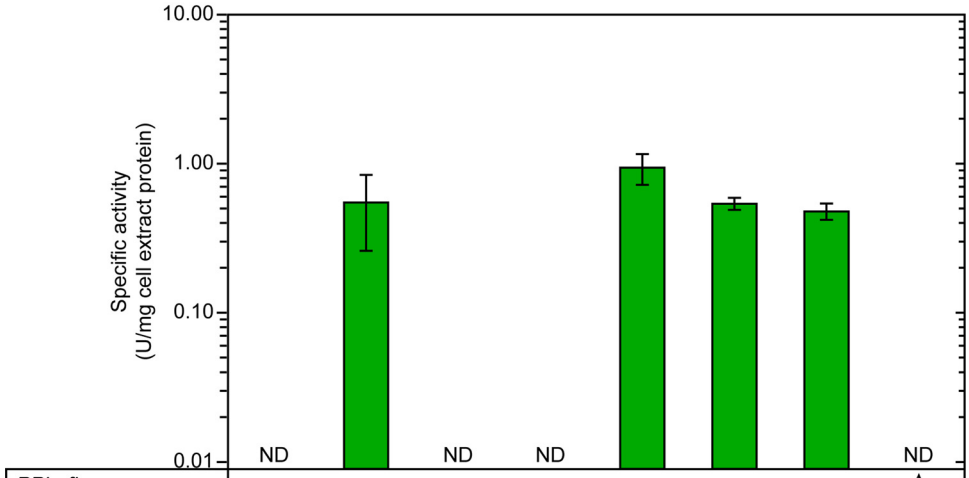

PPi-pfk								Δ
ATP-pfk expressed		+					+	+
tal (*T.sacch*)		+			+	+	+	Δ
ldh				Δ	Δ	Δ	Δ	Δ
T. sacch pyruvate to ethanol pathway		+	+	+	+	+	+	+
Organism	*C. therm*	*T. sacch*	*C. therm*	*C. therm*	*C. therm*	*C. therm*	*C. therm*	*C. therm*
Strain	LL1004	LL1025	LL1570	LL1592	LL1647	LL1648	LL1649	LL1660

FIG 1 Transaldolase (TAL) specific activities of strains used in this study. "ND" indicates that transaldolase activity was not detected, i.e., it was below our limit of detection (<0.01 U/mg cell extract protein). *Cth*, *C. thermocellum*; *Tsac*, *T. saccharolyticum*. The "+" signs indicate the presence of a genetic feature, and the "Δ" sign indicates that a gene is deleted. Strain LL1004 is WT *C. thermocellum* and is a negative control for TAL activity. Strain LL1025 is WT *T. saccharolyticum* and is a positive control for TAL activity. Error bars represent 1 standard deviation ($n \geq 3$).

PFK activity with ATP-linked activity was to decouple glycolysis from the nonoxidative pentose phosphate pathway (PPP) by eliminating the need for SBP activity. To this end, the transaldolase gene from *T. saccharolyticum*, *Tsac_0327*, and its promoter were integrated immediately downstream of the *PP$_i$-pfk* gene. Enzyme assays confirmed that the resulting strain, LL1647, had gained transaldolase activity levels that were comparable to those in *T. saccharolyticum* cell extracts (Fig. 1).

Toxicity of heterologous expression of ATP-*pfk*. Since *C. thermocellum* only grows on C6 sugars and sugar polymers and exclusively uses glycolysis for substrate assimilation, the PFK reaction is essential for growth. Thus, the next step in replacing PP$_i$-*pfk* with ATP-*pfk* was heterologous expression of an ATP-*pfk* gene. Initial attempts to express the *T. saccharolyticum* ATP-*pfk* used the strong constitutive *Clo1313_2638* promoter (25) to drive *ATP-pfk* expression. It was observed that the expression plasmid failed to give transformants despite positive controls obtaining colony counts (see Table S1 in the supplemental material) comparable to previously reported values (26). A no-promoter control *ATP-pfk* expression plasmid (pLL1383) could be transformed into wild-type *C. thermocellum* at an efficiency similar to that of an empty vector, indicating that the lack of transformants with the promoter-containing *ATP-pfk* expression plasmid was linked to expression and thus activity of the ATP-*pfk* gene, and not due to the sequence of the ATP-*pfk* gene.

To reduce toxicity of ATP-*pfk* expression, we engineered the ribosome binding site (RBS) to create plasmids with different predicted translation initiation rates (27) for the *T. saccharolyticum ATP-pfk* gene (Table 2). Lower predicted translation initiation rates allowed us to observe transformants in wild-type *C. thermocellum* (see Table S1); however, when these transformants were assayed for PFK activity, ATP-PFK activities were still below our limit of detection (<0.01 U/mg cell extract protein; see Table S1).

Simultaneous expression of *ATP-pfk* and deletion of *PP$_i$-pfk*. The apparent toxicity of a heterologous ATP-Pfk in *C. thermocellum* needed to be addressed. One possible

TABLE 2 Plasmids used in this study

Plasmid	Description	Accession no.	Source or reference
pDGO143	*C. thermocellum* expression vector	KX259110	26
pLL1381	pDGO143 with *C. thermocellum* Clo1313_2638 promoter driving *T. saccharolyticum ATP-pfk*; native RBS with predicted translation initiation rate of ~95,000 arbitrary units	ON809502	This study
pLL1382	pDGO143 with *C. thermocellum* Clo1313_2638 promoter driving *T. saccharolyticum ATP-pfk*; modified RBS with predicted translation initiation rate of ~500 arbitrary units	ON809503	This study
pLL1383	pDGO143 with *T. saccharolyticum ATP-pfk*; no promoter driving *ATP-pfk* expression	ON809504	This study
pLL1384	pDGO143 with *C. thermocellum* Clo1313_2638 promoter driving *T. saccharolyticum ATP-pfk*; modified RBS with predicted translation initiation rate of ~4,000 arbitrary units	ON809505	This study
pLL1385	pDGO143 with *C. thermocellum* Clo1313_2638 promoter driving *T. saccharolyticum ATP-pfk*; modified RBS with predicted translation initiation rate of ~8,000 arbitrary units	ON809506	This study
pLL1386	pDGO143 with *C. thermocellum* Clo1313_2638 promoter driving *T. saccharolyticum ATP-pfk*; modified RBS with predicted translation initiation rate of ~14,000 arbitrary units	ON809507	This study
pLL1387	pDGO143 with *C. thermocellum* Clo1313_2638 promoter driving *T. saccharolyticum ATP-pfk*; modified RBS with predicted translation initiation rate of ~27,000 arbitrary units	ON809508	This study
pLL1388	Integration vector; introduces *T. saccharolyticum* transaldolase and its native promoter immediately downstream of *C. thermocellum* PP_i*-pfk* gene	ON809509	This study
pLL1389	Integration vector; introduces *T. saccharolyticum* ATP-phosphofructokinase downstream of *Clo1313_0718* (putative ADP-glucose synthase), with a spacer sequence between *Clo1313_0718* and the *ATP-pfk*	ON809510	This study
pLL1390	Replacement vector; deletes *Clo1313_0717-0718* and the spacer sequence, and replaces it with the *T. saccharolyticum ATP-pfk* promoter sequence	ON809511	This study
pLL1391	Deletion vector; deletes *C. thermocellum* PP_i*-pfk*. In strain LL1647 and its derivatives, this plasmid also deletes the previously introduced *T. saccharolyticum* transaldolase	ON809512	This study
pLL1392	Deletion vector; deletes *C. thermocellum* PP_i*-pfk* only in strain LL1647 and its derivatives	ON809513	This study

explanation included the creation of a futile cycling reaction between an ATP-Pfk and PP_i-Pfk, with net result being conversion of ATP to PP_i. However, since *C. thermocellum* does not have a cytosolic pyrophosphatase activity that would hydrolyze the PP_i from this cycling reaction—which would result in ATP wastage—we considered alternatives.

A second and more likely explanation was that expression of ATP-Pfk in *C. thermocellum* shifted cofactor usage at the PFK reaction away from PP_i to ATP, thus reducing the glycolytic demand for PP_i as a phosphoryl donor. Given that PP_i in *C. thermocellum* comes from both biosynthesis and primarily from a nonbiosynthetic reaction, the reduced demand for PP_i from the PFK reaction would result in accumulation of PP_i in the cell, as the nonbiosynthetic reaction continues to generate PP_i. The effect of PP_i accumulation would be inhibition of biosynthetic reactions, leading to arrest in cell growth (28). This therefore suggested that expression of ATP-*pfk* is conditional on disruption of the nonbiosynthetic PP_i mechanism, so that PP_i accumulation could be mitigated.

Since our initial approach of sequentially expressing a heterologous ATP-*pfk* gene failed, we devised a two-step strategy to allow for simultaneous activation of ATP-*pfk* expression and disruption of PP_i generation. It was previously reported that there were several candidates for PP_i generation in *C. thermocellum*, of which two were believed to be the likely sources: the membrane-bound pyrophosphatase encoded by the gene *Clo1313_0823*, and the ADP-glucose synthase enzyme complex encoded by the two-gene operon, *Clo1313_0717-0718* (10, 11). Since it has previously been reported that both the membrane-bound pyrophosphatase (*Clo1313_0823*) gene (20) and the *ppdk* gene (10) could be deleted from *C. thermocellum*, we hypothesized that the APD-glucose synthase enzyme complex (used for glycogen cycling) was the likely candidate for PP_i generation. In the first step, the *T. saccharolyticum* ATP-*pfk* was integrated immediately downstream of the ADP-glucose synthase operon (*Clo1313_0717-0718*) (see Fig. S1). To avoid unintended ATP-PFK activity due to unwanted translation of this ATP-*pfk* gene, a spacer sequence was included between the ADP-glucose synthase operon and the *T. saccharolyticum* ATP-*pfk* coding sequence, with the predicted effect of significantly reducing the translation rate of the ATP-*pfk* gene. In the second step, the ADP-

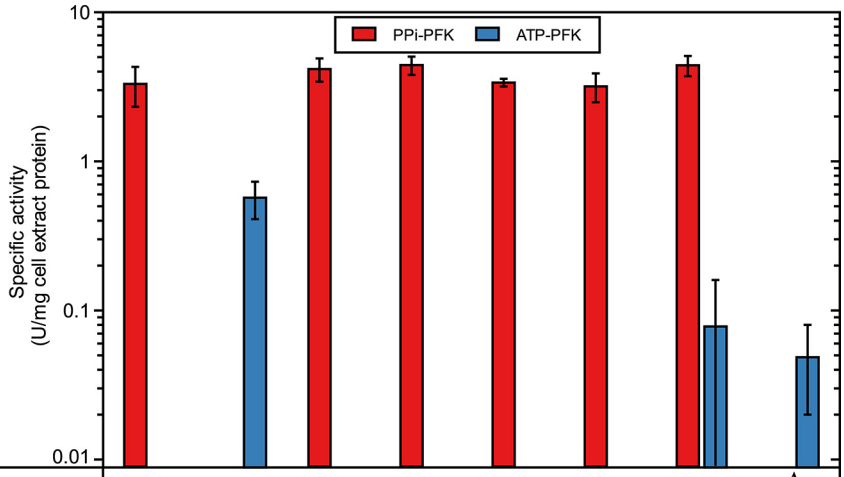

PPi-*pfk*								Δ
ATP-*pfk* expressed		+					+	+
tal (*T. sacch*) expressed		+			+	+	+	Δ
ldh				Δ	Δ	Δ	Δ	Δ
T. sacch pyruvate to ethanol pathway		+	+	+	+	+	+	+
Organism	*C. therm*	*T. sacch*	*C. therm*	*C. therm*	*C. therm*	*C. therm*	*C. therm*	*C. therm*
Strain	LL1004	LL1025	LL1570	LL1592	LL1647	LL1648	LL1649	LL1660

FIG 2 PFK activities for strains used in this study, with PP_i (red) or ATP (blue) as the cofactor. Where there is no column plot, PFK activity was below the limit of detection (<0.01 U/mg cell extract protein). The "+" signs indicate the presence of a genetic feature, and the "Δ" sign indicates that a gene is deleted. Strain LL1004 is WT *C. therm*(*ocellum*) and is a negative control for ATP-PFK activity, and a positive control for PP_i-PFK activity. Strain LL1025 is WT *T. sacch*(*arolyticum*), and is a positive control for ATP-PFK activity and a negative control for PP_i-PFK activity. Error bars represent 1 standard deviation ($n \geq 3$).

glucose synthase operon, as well as the insertion sequence, was replaced by the *T. saccharolyticum* ATP-*pfk* promoter sequence, thus simultaneously removing ADP-glucose synthase (the hypothesized PP_i-generating mechanism), and expressing ATP-*pfk* (see Fig. S1) to ensure that PFK activity was complemented prior to deleting the PP_i-*pfk*. Gain of ATP-PFK activity in the resulting strain (LL1649) was confirmed by detection of low ATP-PFK activity (~0.08 U/mg cell extract protein) in cell extracts of strain LL1649 (Fig. 2). While the ATP-PFK activity observed in strain LL1649 was much lower than that in *T. saccharolyticum* cell extracts (~0.57 U/mg cell extract protein), it was still greater than that of non-ATP-PFK-expressing strains, where ATP-PFK was below the limit of detection (<0.01 U/mg cell extract protein). Analysis of relative gene expression levels revealed that ATP-*pfk* expression in strain LL1649 was comparable to that in *T. saccharolyticum* (see Fig. S2). Proteomic analyses of strains LL1649 and wild-type *T. saccharolyticum* subsequently confirmed that the relative protein abundance of ATP-Pfk protein was ~10-fold lower in strain LL1649 than in *T. saccharolyticum* (see Fig. S3), consistent with the observed difference in enzyme activity (Fig. 2). The simplest way to reconcile these observations is that ATP-Pfk expression is limited at the level of translation.

After successfully achieving chromosomal expression of ATP-*pfk*, we proceeded to delete the native PP_i-*pfk* gene. Two plasmids were used; one to delete only the PP_i-*pfk* coding sequence (pLL1392), and the other to delete both the PP_i-*pfk* coding sequence, as well as the *T. saccharolyticum* transaldolase expression cassette that had originally been introduced (pLL1391). We expected that deletion of the transaldolase would not be possible due to its anticipated essential role (see Introduction); however, the deletion attempt using plasmid pLL1391 worked, resulting in a strain that had neither PP_i-*pfk* nor transaldolase (strain LL1660). The deletions were confirmed both by loss of PP_i-PFK (Fig. 2) and TAL (Fig. 1) activities in strain LL1660.

Investigating changes to thermodynamic driving force of the PFK reaction. To determine whether replacing the *C. thermocellum* PP_i-*pfk* with a heterologous *ATP-pfk* leads

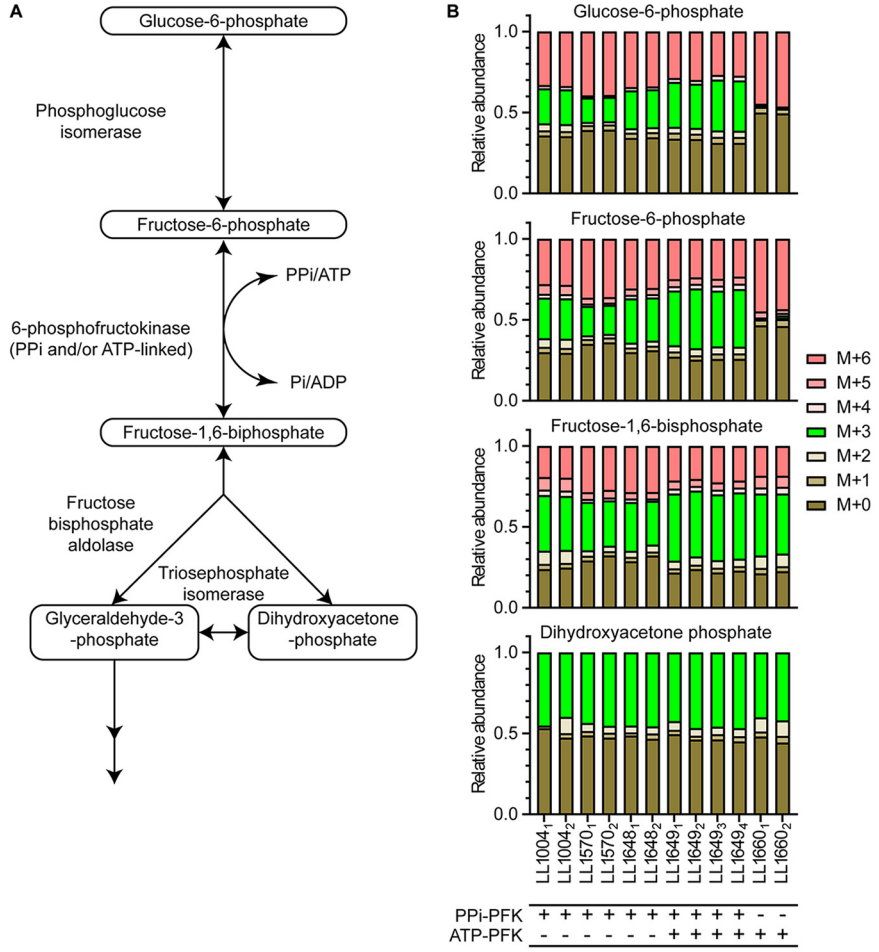

FIG 3 (A) Metabolic diagram of glycolysis around the PFK reaction and the enzymes that catalyze the reactions. (B) ^{13}C-labeling patterns for key glycolytic metabolites (glucose-6-phosphate, fructose-6-phosphate, fructose-1,6-bisphosphate, and dihydroxyacetone phosphate) for cells fed a 50:50 mixture of uniformly labeled and naturally labeled glucose. The "M+" notation indicates the number of ^{13}C-labeled carbon atoms (i.e., M+6 indicates six labeled carbon atoms). The subscript after the strain ID number indicates biological replicate number. The cofactor specificity of the PFK reaction is indicated below the strain name: "+" indicates the presence of a reaction, and "−" indicates the absence of a reaction.

to greater thermodynamic driving force in glycolysis, *C. thermocellum* strains were cultured on a 50:50 ratio of naturally and uniformly ^{13}C-labeled cellobiose ([U-$^{13}C_{12}$]cellobiose). As previously described (8), the forward PFK reaction will produce a 50:50 mixture of unlabeled and fully labeled fructose-1,6-bisphosphate (FBP), in turn producing dihydroxyacetone phosphate (DHAP) and glyceraldehyde-3-phosphate (G3P) in a similar 50:50 ratio of unlabeled to labeled. However, reverse flux of the fructose bisphosphate aldolase has a 50% chance to produce M+3-labeled FBP (FBP_{M+3}; i.e., with three ^{13}C carbon atoms) from this mixed pool of G3P and DHAP; the FBP_{M+3} in turn can be converted to M+3-labeled fructose-6-phosphate ($F6P_{M+3}$) by reverse PFK flux and then to M+3 glucose-6-phosphate (G6P) by reverse phosphoglucose isomerase flux (Fig. 3A). The relative abundance of the M+3 isotopomer in the F6P pool therefore gives an indication of the reverse flux through the PFK reaction. A smaller ratio of $F6P_{M+3}$ versus FBP_{M+3} would therefore represent a less reversible PFK reaction, which in turn would suggest a more thermodynamically favorable forward PFK reaction (9).

It was observed that the relative abundance of the M+3 fractions for both G6P and F6P were more or less similar among wild-type *C. thermocellum* and engineered *C. thermocellum* strains that still contained the PP_i-*pfk* gene (Fig. 3B); the ratios observed for the M+3 F6P and G6P were similar to previously reported results (8). Strains with both

PP_i-*pfk* and ATP-*pfk* genes (LL1649) showed an M+3 labeling pattern similar to that of the wild type. Deletion of the PP_i-*pfk* to create strain a strain with only ATP-PFK activity (LL1660) substantially reduced the M+3 G6P and F6P fractions, suggesting that switching the cofactor usage of the PFK reaction from PP_i to ATP decreased the reversibility of the PFK reaction in *C. thermocellum*.

The M+3-labeled fraction is not observed in glucose-1-phosphate (G1P) (see Fig. S4). Since phosphoglucomutase is present in *C. thermocellum* (29), and the reaction is close to equilibrium under standard conditions ($\Delta G'° = 0.8$ kJ/mol [12]), the lack of reversibility of this reaction suggests that it is actively regulated.

In comparing metabolite pool sizes across the different samples, we further observe that expression and replacement of the PP_i-*pfk* gene with an ATP-*pfk* gene (strain LL1660) resulted in a significant decrease in the F6P pool size, and a corresponding increase in the FBP pool size (Fig. 4), resulting in a much greater FBP/F6P ratio than strains that still contained the more reversible PP_i-PFK pathway, making the FBP/F6P pool ratios of this *C. thermocellum* strain more similar to that of organisms with a canonical glycolysis pathway, such as *E. coli* (30) and *T. saccharolyticum* (8). Other significant changes to metabolite pool sizes include a transient increase in pyruvate concentrations when both PP_i-*pfk* and ATP-*pfk* were present (strain LL1649) and a decrease in the ATP pool once all PFK activity was ATP-linked (strain LL1660).

Effect on fermentation. The engineered strains in this study were cultured on 60 g/L cellobiose in defined medium to determine whether replacing PP_i-*pfk* with ATP-*pfk* affected the quantity or distribution of fermentation products. Consumption of cellobiose and production of glucose, ethanol, and acetate (the primary fermentation products in the parent strain) were largely unaffected. A slight increase in biomass production (measured by pellet nitrogen) was observed upon deletion of the PP_i-*pfk* gene (strain LL1660) (Fig. 5).

Resequencing analyses. Whole-genome resequencing confirmed the presence of the various modifications in the strains created in this study (see File S3 in the supplemental material). In particular, it confirmed that ADP-glucose synthase was deleted and replaced by the *T. saccharolyticum* ATP-*pfk* promoter in strain LL1649 (as intended) and that this feature was preserved in strain LL1660 when both PP_i-*pfk* and transaldolase were deleted.

We observed a partial genome duplication in strain LL1660 and three of its sister colonies (LL1661, LL1662, and LL1663) (see Fig. S5). The evidence for the gene duplication is that read depth is approximately doubled along the length of the region compared to the parent strain. The presence of a repeated insertion element at each end of the duplicated region suggests that the duplication was mediated by homologous recombination. Included in the duplicated region are the CDSs *Clo1313_0790* to *Clo1313_1248*. This region includes several genes that may play a role in energy metabolism and cofactor cycling, including a putative native ATP-*pfk* gene (Clo1313_0997), the *pta-ack* pathway (Clo1313_1185-1186), the membrane-bound pyrophosphatase (Clo1313_0823), and the pyruvate phosphate dikinase gene (Clo1313_0949); however, the effect of the gene duplication on these activities was not investigated since its extent meant there was an impractical number of avenues of investigation to tackle in one study. One practical implication of this chromosome duplication event is to make it significantly more difficult to perform subsequent chromosomal modifications in this region due to the presence of two copies of each gene and potential for additional unintended recombination events.

DISCUSSION

The absence of transaldolase in *C. thermocellum* has led to speculation that this organism uses a variant of the PPP, where SBP-to-S7P conversion is necessary for the efficient generation of C5 compounds, and that this reaction is mediated by the PP_i-Pfk enzyme (7, 21, 22). This was the motivation for introducing a transaldolase gene from *T. saccharolyticum* before deleting the PP_i-*pfk* gene. However, the creation of a strain lacking both transaldolase and PP_i-*pfk* suggests that our previous hypothesis about the pathway for C6-to-C5 interconversion was wrong. The pathway for interconversion of

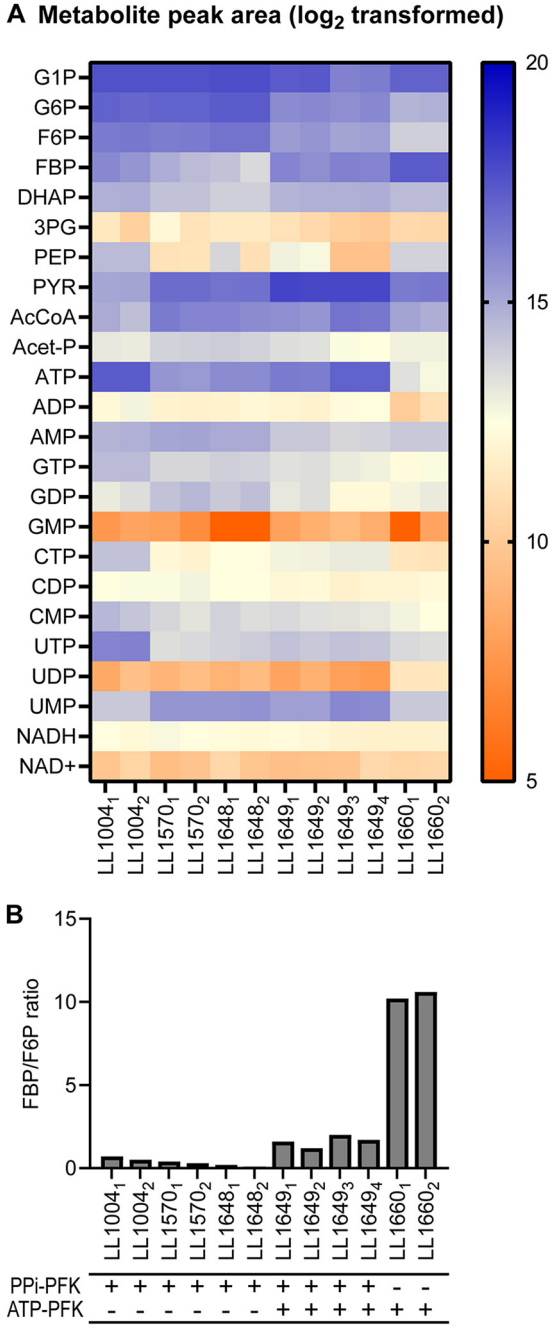

FIG 4 (A) Comparison of log_2-transformed peak area values for glycolytic metabolites. (B) FBP/F6P ratios for the different samples. Subscripts after the strain ID number indicates replicate number. The cofactor specificity of the PFK reaction is indicated below the strain name: the "+" indicates the presence of a reaction, and "−" indicates the absence of a reaction.

pentose and hexose sugars in this strain is not known. One possibility is that *C. thermocellum* has alternate means for interconverting hexoses and pentoses; one such pathway is the L-type pentose phosphate pathway (31), where octulose phosphates play an intermediary role for conversion between hexose phosphates and pentose phosphates. Further study will be needed to determine whether such a pathway operates in *C. thermocellum*.

Why was introducing the ATP-*pfk* gene so difficult? Initially, we suspected that simultaneous presence of both ATP-linked and PP_i-linked PFK activity would be toxic. Since PP_i-PFK activity is reversible, it presents the opportunity for a futile cycle where

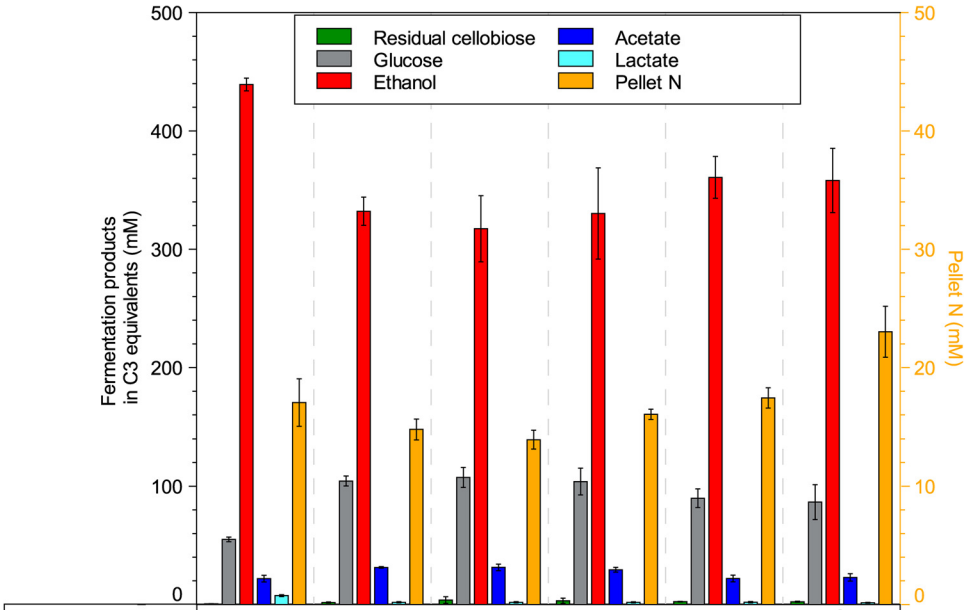

PPi-*pfk*						Δ
ATP-*pfk* expressed					+	+
Transaldolase			+	+	+	Δ
ldh		Δ	Δ	Δ	Δ	Δ
T. sacch pyruvate to ethanol pathway	+	+	+	+	+	+
Strain	LL1570	LL1592	LL1647	LL1648	LL1649	LL1660

FIG 5 Fermentation product profiles for the *C. thermocellum* strains in this study. Note that concentrations for the fermentation products are reported in C3 sugar equivalents. The "+" sign indicates introduction of a genetic feature, and the "Δ" sign indicates deletion of a genetic feature. Error bars represent 1 standard deviation ($n \geq 3$).

ATP-PFK converts F6P to FBP and PP_i-PFK converts FBP to F6P, resulting in a net conversion of ATP + P_i → ADP + PP_i. Indeed, in organisms that use fructose bisphosphatase (FBP; EC 3.1.3.11) for gluconeogenesis, the activities of FBP and PFK are regulated to ensure that only one is active (32). However, the successful generation of a strain where both activities are present (LL1649) eliminates that hypothesis. Furthermore, in that strain, ATP levels are similar to that of the wild-type strain (LL1004) (Fig. 4), indicating that if any futile cycling is happening, the flux is low enough that it does not significantly affect the adenylate pool. In other organisms, such as *E. coli*, PP_i-*pfk* genes have been heterologously induced and expressed—for the purposes of purifying said PP_i-Pfk proteins—alongside the native putative ATP-*pfk* (22, 33–36), further casting doubt on the futile cycling hypothesis.

One of the most significant metabolic impacts of the expression of ATP-*pfk* was an increase in the FBP pool. FBP is known to regulate many enzymes. In *C. thermocellum* cell extract, the addition of FBP has been shown to effectively abolish glycolytic flux (37). However, this would not explain the need to disrupt glycogen cycling in order for ATP-*pfk* expression to succeed.

The most likely explanation is that the introduction of ATP-*pfk* caused an increase in PP_i levels, and eliminating the PP_i generated by glycogen cycling (by deleting the ADP-glucose synthase reaction) was necessary to eliminate excess PP_i. Although many organisms have a cytosolic pyrophosphatase to eliminate excess PP_i, *C. thermocellum* does not (20). PP_i levels are known to regulate the activity of both the pyruvate phosphate dikinase (Ppdk) and malic enzymes (38). The stimulatory role of decreasing PP_i levels is also consistent with cell extract experiments (F6P stimulates flux, but FBP inhibits it) (37). Although many factors are still unknown regarding the role of PP_i in

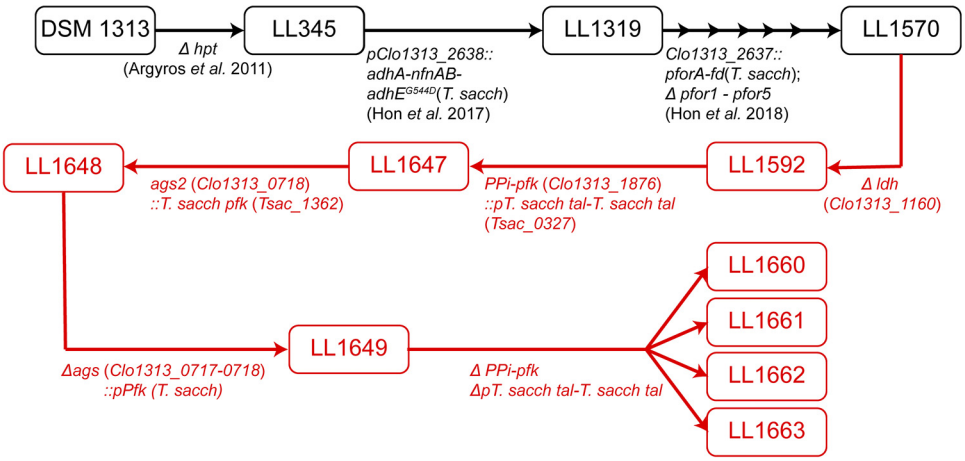

FIG 6 Diagram of strain lineage. Strains shown in black are previously reported in literature. Strains in red were created in this study. Modifications that occurred between strains are listed below their respective arrows. Multiple arrows indicate several sequential modifications.

C. thermocellum metabolism, the strains developed here provide a new and exciting avenue for testing hypotheses.

A surprising finding of this work was the extremely localized result of replacing the PP_i-*pfk* gene with ATP-*pfk* gene. Our current understanding of *C. thermocellum* metabolism is that it operates close to thermodynamic equilibrium (8). Therefore, we would expect the introduction of a reaction with a high thermodynamic driving force (such as ATP-PFK) to deplete upstream metabolite pools and expand downstream ones. We found that this was, in fact, the case—at least for the metabolites immediately adjacent to the PFK reaction. However, this effect extended upstream only to G6P, and there was almost no effect on DHAP levels. This suggests active regulation of other reactions in glycolysis, or that the metabolic pathways downstream of PFK cannot carry the additional flux. The localized effect of this change further explains why the titer and distribution of fermentation products was largely unaffected.

MATERIALS AND METHODS

Strain and plasmid construction. Figure 6 shows how the relationships among the strains used in this study; Table 1 provides full details for all strains used in this study. Plasmids used in this study are listed in Table 2; all plasmids were constructed via isothermal assembly (39), using a commercial kit from New England Biolabs (NEBuilder HiFi DNA Assembly Master Mix, catalog number E2621). Purification of DNA (plasmid or PCR products) was done with commercially available kits from Zymo Research and New England Biolabs. Transformation of *C. thermocellum* was performed as previously described (40); plasmid DNA that was to be transformed into *C. thermocellum* was purified from *Escherichia coli* BL21 derivative strains (New England Biolabs catalog number C2566) to ensure proper methylation of the plasmid DNA (41).

Media preparation and culture conditions. All reagents used in this study were of molecular grade, and obtained from Sigma-Aldrich or Fisher Scientific, unless otherwise noted.

C. thermocellum and *T. saccharolyticum* strains were grown at 55°C under anaerobic conditions, either in tubes when grown in anaerobic chambers (Coy Laboratory Products, Grass Lakes, MI), with previously described environmental conditions (23), or in sealed serum bottles prepared as previously described (23).

Complex medium CTFUD was prepared as previously described (40); this medium was used for culturing *C. thermocellum* cells that were to be used in transformations or for preparing genomic DNA for strain resequencing. Defined medium MTC-5 was prepared as previously described (23) and was used for all other purposes. *T. saccharolyticum* cells (used to generate cell extracts of this bacterium for use in enzyme assays) were grown in MTC-6 medium (42).

Determination of transformation efficiencies. Transformation efficiencies of the ATP-*pfk* expression plasmids was determined as previously described (26) by plating serial dilutions of recoveries and then counting the number of CFU where the dilution allowed for clear differentiation of *C. thermocellum* colonies. Transformation efficiency was determined from two independent transformations of the plasmids into wild-type *C. thermocellum*.

(i) Enzyme assays. Cells to be used for enzyme assays were grown, harvested, and lysed to obtain cell extract as previously described (23). Protein concentrations were determined using the Bradford protein dye assay (Bio-Rad, catalog number 1856210), with bovine serum albumin used as a protein standard. All enzyme assays were performed at 55°C under anaerobic conditions.

(ii) Transaldolase assay. Transaldolase activity was assayed by measuring the formation of glyceraldehyde-3-phosphate as previously described (43). The assay reaction was slightly modified from previously described (43), and contained 100 mM Tris-HCl (pH 8.0), 5 mM $MgCl_2$, 0.3 mM NADH, 1 mM erythrose-4-phosphate, 1 mM fructose-6-phosphate, 4 U/mL triosephosphate isomerase, 4 u/mL α-glycerophosphate dehydrogenase, and cell extract. The assay reaction was started with the addition of fructose-6-phosphate.

(iii) 6-Phosphofructokinase assay. The PFK activity was assayed by formation of fructose-1,6-bisphosphate and modified from a previously described method (10). The assay reaction contained 100 mM Tris-HCl, 5 mM $MgCl_2$, 0.15 mM NADH, 1 mM fructose-6-phosphate, 4 U/mL fructose bisphosphate aldolase, 4 U/mL triosephosphate isomerase, 4 U/mL α-glycerophosphate dehydrogenase, cell extract, and 2 mM either PP_i or ATP. The assay reaction was started by the addition of the phosphate donor (PP_i or ATP).

Intracellular metabolite measurements. (i) ^{13}C labeling of *C. thermocellum* intracellular metabolites. *C. thermocellum* was grown on MTC-5 medium, with the main carbon source consisting of 3 mM naturally labeled cellobiose (i.e., unlabeled except for the naturally occurring abundance of ^{13}C carbon atoms), and 3 mM uniformly labeled ^{13}C-cellobiose ([UL-$^{13}C_{12}$]cellobiose), sourced from Omicron Biomedicals, catalog number CEL-002. Then, 8-mL cultures were inoculated with 8 or 0.8 μL of inoculum volume and grown at 55°C under anaerobic conditions. Freezer stocks were prepared by growing cells on MTC-5 with 5 g/L naturally labeled cellobiose to mid-exponential phase (optical density at 600 nm [OD_{600}] of ~0.6 at the time the stocks were made).

Metabolite samples were harvested when the cells were growing at mid-exponential phase (OD_{600} ~0.5); to ensure that total metabolites extracted were similar across different cultures, the volume of culture to be harvested in milliliters was determined by dividing 2.5 by the OD_{600} value at the time of harvesting, i.e., ~5 mL of culture was harvested when the OD_{600} of the culture was ~0.5. Intracellular metabolites were collected as previously described (8) by vacuum filtering a culture through a 0.45-μm hydrophilic nylon filter to separate cells from medium. The filters were then placed in 1.6 mL of cold (−80°C) metabolite extraction solvent (40% methanol, 40% acetonitrile, 20% water) cell-side down. Cells were washed off the filter using the extraction solvent, and then metabolites were separated from cellular debris by centrifugation (8, 44). Metabolite samples were kept at −80°C when not used.

(ii) Analyses of *C. thermocellum* metabolite samples via LC-MS. Metabolite samples were analyzed by liquid chromatography-mass spectrometry (LC-MS) as described previously (8). Samples were dried under N_2 gas and resuspended in solvent A (97:3 H_2O-methanol with 10 mM tributylamine adjusted to pH 8.2 by the addition of acetic acid to an ~10 mM final concentration). Solvent B was 100% methanol, and the following gradient was used for chromatographic separation: 0 to 2.5 min, 5% B; 2.5 to 17 min, linear gradient from 5 to 95% B; 17 to 19.5 min, 95% B; 19.5 to 20 min, linear gradient from 95 to 5% B; and 20 to 25 min, 5% B. Separation was achieved on a 2.1 × 100-mm Acquity ultra-high-pressure liquid chromatography ethylene bridge hybrid (UHPLC BEH) C_{18} column with a 1.7-μm particle size (Waters) at 25°C on a Vanquish UPLC coupled to a Q Exactive mass spectrometer (Thermo Scientific) by an electrospray ionization (ESI) source operating in negative mode. Mass spectrometry parameters were full MS-SIM (single ion-monitoring) scanning from 70 to 1,000 *m/z*, a resolution of 70,000 full width at half maximum (FWHM), a maximum injection time (IT) of 40 ms, and an automatic control gain (ACG) target of 1e6. Data were analyzed using the MAVEN software suite (45, 46), and compounds were identified by monoisotopic mass and retention time matching to pure standards. File S1 in the supplemental material contains data for ^{13}C labeling of intracellular metabolites, as well as the relative metabolite abundance.

Fermentation product analyses. Fermentation product analyses was done as previously described (1), with the modification of using 60 g/L cellobiose as the main carbon source instead of 50 g/L to ensure that ethanol titer was not limited by substrate concentration. Fermentations were performed in anaerobic sealed serum bottles with the headspace purged with 100% nitrogen and were cultured at 55°C for 168 h (7 days) before they were sampled for analyses.

Fermentation products were quantified by high performance liquid chromatography as previously described (47). Headspace composition in serum bottles was determined as previously described. Pellet nitrogen (used as a proxy for cell biomass) was measured as previously described (48).

Gene expression analyses. Measuring the expression of the *T. saccharolyticum* ATP-*pfk* and *C. thermocellum* PP_i-*pfk* was done via reverse transcriptase quantitative PCR (RT-qPCR) as previously described (26). The primers used for qPCR are reported in Table 3. ATP-*pfk* expression in each strain was normalized against the expression of the *recA* reference gene (49) to allow for comparison across different strains and species.

Proteomics analyses. Cells for proteomic analyses were cultured on defined MTC-5 or MTC-6 medium, depending on bacterial species, and harvested at mid-exponential phase ($n = 3$). Cells were pelleted, washed, and then processed for LC-MS/MS-based proteomic analyses as previously described (50). For each sample, 3-μg portions of tryptic peptides were loaded, separated, and analyzed by one-dimensional LC-MS/MS using a Vanquish uHPLC plumbed directly in-line with a Q Exactive Plus mass spectrometer (Thermo Scientific) operating in data-dependent acquisition. Tandem mass spectra were searched against the relevant *C. thermocellum* and *T. saccharolyticum* proteome databases using Proteome Discoverer v.2.3 and informatically postprocessed, as previously described (51).

Protein abundance raw and normalized data are provided in File S2 in the supplemental material.

Sequencing and resequencing analyses. Routine Sanger sequencing of plasmids and PCR products was performed by Genewiz, Inc. (NJ, USA), with a minimum 2-fold coverage of sequences. Whole-genome resequencing was performed by the Department of Energy Joint Genome Institute using the Illumina MiSeq sequencing platform, with minimum 100-fold coverage. Strains were analyzed with the software CLC Genomics Workbench (Qiagen) using strain DSM1313 as the reference genome (GenBank accession

TABLE 3 Primers used for RT-qPCR

Primer	Target (species, gene, primer orientation)	Sequence (5′–3′)
XSH0367	*C. thermocellum*, PP_i*-pfk*, forward	ATGCATATTCGGACAATCC
XSH0905	*C. thermocellum*, PP_i*-pfk*, reverse	TGAGCTGCTCCGTAAACTGC
XSH0901	*T. saccharolyticum*, *ATP-pfk*, forward	TAGAGACACGGCAACGTCAC
XSH0902	*T. saccharolyticum*, *ATP-pfk*, reverse	ATAATCTCTGCTCCTCCAGC
XSH0198	*C. thermocellum*, *recA*, forward	TTTACGGCCAGGGTATTTCA
XSH0199	*C. thermocellum*, *recA*, reverse	GCCAATCTTCTGACCGTTGT
XSH0200	*T. saccharolyticum*, *recA*, forward	GAAGCCTTAGTGCGAAGTGG
XSH0201	*T. saccharolyticum*, *recA*, reverse	GAAGTCCAACATGTGCATCG

NC_017304.1); reads were filtered against strain LL1570 (accession number SRP144049) (1) to exclude inherited mutations. A summary of the identified mutations is provided in File S3 in the supplemental material.

Data availability. Whole-genome resequencing data for the strains in this study were deposited in the NCBI Sequence read archive under the accession numbers listed in Table 1. Plasmid sequence accession numbers are listed in Table 2. Raw LC/MS data for metabolite samples were deposited in Zenodo (10.5281/zenodo.7032172).

SUPPLEMENTAL MATERIAL

Supplemental material is available online only.

SUPPLEMENTAL FILE 1, PDF file, 1 MB.

SUPPLEMENTAL FILE 2, XLSX file, 0.1 MB.

SUPPLEMENTAL FILE 3, XLSX file, 0.8 MB.

SUPPLEMENTAL FILE 4, XLSX file, 0.02 MB.

ACKNOWLEDGMENTS

Funding was provided by The Center for Bioenergy Innovation, a U.S. Department of Energy (DOE) Research Center supported by the Office of Biological and Environmental Research in the DOE Office of Science. Whole-genome resequencing was performed by the DOE Joint Genome Institute, a DOE Office of Science User Facility, and is supported by the Office of Science of the U.S. DOE under contract DE-AC02-05CH11231.

L.R.L. is a founder of Enchi Corporation, which has a financial interest in engineering *C. thermocellum*. S.H. is an employee of Enchi corporation.

S.H. and D.G.O. designed the experiments. S.H. performed strain and plasmid construction, biochemical assays, gene expression measurements, fermentations and subsequent analyses, generating metabolite samples in labeling experiments, and analyses of Sanger sequencing and whole-genome resequencing. T.J. and D.M.S. performed the analyses of *C. thermocellum* metabolite samples. R.J.G. and R.L.H. performed proteomic analyses of *C. thermocellum* and *T. saccharolyticum*. M.I.M. prepared whole-genome resequencing samples. S.H., D.G.O., T.J., and R.J.G. wrote the manuscript. D.A.-N., D.G.O., and L.R.L. revised the manuscript.

REFERENCES

1. Hon S, Holwerda EK, Worthen RS, Maloney MI, Tian L, Cui J, Lin PP, Lynd LR, Olson DG. 2018. Expressing the *Thermoanaerobacterium saccharolyticum pforA* in engineered *Clostridium thermocellum* improves ethanol production. Biotechnol Biofuels 11:242. https://doi.org/10.1186/s13068-018-1245-2.
2. Tian L, Papanek B, Olson DG, Rydzak T, Holwerda EK, Zheng T, Zhou J, Maloney M, Jiang N, Giannone R, Hettich R, Guss A, Lynd L. 2016. Simultaneous achievement of high ethanol yield and titer in *Clostridium thermocellum*. Biotechnol Biofuels 9:116. https://doi.org/10.1186/s13068-016-0528-8.
3. Mazzoli R, Olson DG. 2020. *Clostridium thermocellum*: a microbial platform for high-value chemical production from lignocellulose. Adv Appl Microbiol 113:111–161. https://doi.org/10.1016/bs.aambs.2020.07.004.
4. Holwerda EK, Olson DG, Ruppertsberger N, Stevenson DM, Murphy SJ-L, Maloney MI, Lanahan AA, Amador-Noguez D, Lynd LR. 2020. Metabolic and evolutionary responses of *Clostridium thermocellum* to genetic interventions aimed at improving ethanol production Metabolic and evolutionary responses of *Clostridium thermocellum* to genetic interventions aimed at improving ethanol production. Biotechnol Biofuels 13:40. https://doi.org/10.1186/s13068-020-01680-5.
5. Dien BS, Cotta MA, Jeffries TW. 2003. Bacteria engineered for fuel ethanol production: current status. Appl Microbiol Biotechnol 63:258–266. https://doi.org/10.1007/s00253-003-1444-y.
6. Lynd LR, Weimer PJ, Van Zyl WH, Pretorius IS. 2002. Microbial cellulose utilization: fundamentals and biotechnology. Microbiol Mol Biol Rev 66:506–577. https://doi.org/10.1128/MMBR.66.3.506-577.2002.
7. Taillefer M, Sparling R. 2016. Glycolysis as the central core of fermentation. Adv Biochem Eng Biotechnol 156:55–77. https://doi.org/10.1007/10_2015_5003.
8. Jacobson TB, Korosh TC, Stevenson DM, Foster C, Maranas CD, Olson DG, Lynd LR, Amador-Noguez D. 2020. *In vivo* thermodynamic analysis of glycolysis in *Clostridium thermocellum* and *Thermoanaerobacterium saccharolyticum* using ^{13}C and ^{2}H tracers. mSystems 5:e00736-19. https://doi.org/10.1128/mSystems.00736-19.
9. Park JO, Tanner LB, Wei MH, Khana DB, Jacobson TB, Zhang Z, Rubin SA, Li SH-J, Higgins MB, Stevenson DM, Amador-Noguez D, Rabinowitz JD. 2019. Near-equilibrium glycolysis supports metabolic homeostasis and energy yield. Nat Chem Biol 15:1001–1008. https://doi.org/10.1038/s41589-019-0364-9.

10. Zhou J, Olson DG, Argyros DA, Deng Y, van Gulik WM, van Dijken JP, Lynd LR. 2013. Atypical glycolysis in *Clostridium thermocellum*. Appl Environ Microbiol 79:3000–3008. https://doi.org/10.1128/AEM.04037-12.
11. Kuil T, Hon S, Yayo J, Foster C, Ravagnan G, Maranas CD, Lynd LR, Olson DG, van Maris AJA. 2022. Functional analysis of H^+-pumping membrane-bound pyrophosphatase, ADP-glucose synthase, and pyruvate phosphate dikinase as pyrophosphate sources in *Clostridium thermocellum*. Appl Environ Microbiol 88:e01857-21. https://doi.org/10.1128/aem.01857-21.
12. Flamholz A, Noor E, Bar-Even A, Milo R. 2012. eQuilibrator: the biochemical thermodynamics calculator. Nucleic Acids Res 40(Database issue): D770–D775. https://doi.org/10.1093/nar/gkr874.
13. Noor E, Bar-Even A, Flamholz A, Reznik E, Liebermeister W, Milo R. 2014. Pathway thermodynamics highlights kinetic obstacles in central metabolism. PLoS Comput Biol 10:e1003483. https://doi.org/10.1371/journal.pcbi.1003483.
14. Tian L, Cervenka ND, Low AM, Olson DG, Lynd LR. 2019. A mutation in the AdhE alcohol dehydrogenase of *Clostridium thermocellum* increases tolerance to several primary alcohols, including isobutanol, *n*-butanol, and ethanol. Sci Rep 9:1–7. https://doi.org/10.1038/s41598-018-37979-5.
15. Tian L, Perot SJ, Stevenson D, Jacobson T, Lanahan AA, Amador-Noguez D, Olson DG, Lynd LR. 2017. Metabolome analysis reveals a role for glyceraldehyde-3-phosphate dehydrogenase in the inhibition of *C. thermocellum* by ethanol. Biotechnol Biofuels 10:276. https://doi.org/10.1186/s13068-017-0961-3.
16. Park JO, Rubin SA, Xu Y-F, Amador-Noguez D, Fan J, Shlomi T, Rabinowitz JD. 2016. Metabolite concentrations, fluxes and free energies imply efficient enzyme usage. Nat Chem Biol 12:482–489. https://doi.org/10.1038/nchembio.2077.
17. Bennett BD, Yuan J, Kimball EH, Rabinowitz JD. 2008. Absolute quantitation of intracellular metabolite concentrations by an isotope ratio-based approach. Nat Protoc 3:1299–1311. https://doi.org/10.1038/nprot.2008.107.
18. Dash S, Olson DG, Joshua Chan SH, Amador-Noguez D, Lynd LR, Maranas CD. 2019. Thermodynamic analysis of the pathway for ethanol production from cellobiose in *Clostridium thermocellum*. Metab Eng 55:161–169. https://doi.org/10.1016/j.ymben.2019.06.006.
19. Rydzak T, McQueen PD, Krokhin OV, Spicer V, Ezzati P, Dwivedi RC, Shamshurin D, Levin DB, Wilkins JA, Sparling R. 2012. Proteomic analysis of *Clostridium thermocellum* core metabolism: relative protein expression profiles and growth phase-dependent changes in protein expression. BMC Microbiol 12:214. https://doi.org/10.1186/1471-2180-12-214.
20. Holwerda EK, Zhou J, Hon S, Stevenson DM, Amador-Noguez D, Lynd LR, van Dijken JP. 2020. Metabolic fluxes of nitrogen and pyrophosphate in chemostat cultures of *Clostridium thermocellum* and *Thermoanaerobacterium saccharolyticum*. Appl Environ Microbiol 86:e01795-20. https://doi.org/10.1128/AEM.01795-20.
21. Susskind BM, Warren LG, Reeves RE. 1982. A pathway for the interconversion of hexose and pentose in the parasitic amoeba *Entamoeba histolytica*. Biochem J 204:191–196. https://doi.org/10.1042/bj2040191.
22. Koendjbiharie JG, Hon S, Pabst M, Hooftman R, Stevenson DM, Cui J, Amador-Noguez D, Lynd LR, Olson DG, van Kranenburg R. 2020. The pentose phosphate pathway of cellulolytic clostridia relies on 6-phosphofructokinase instead of transaldolase. J Biol Chem 295:1867–1878. https://doi.org/10.1074/jbc.RA119.011239.
23. Hon S, Olson DG, Holwerda EK, Lanahan AA, Murphy SJ, Maloney MI, Zheng T, Papanek BA, Guss AM, Lynd LR. 2017. The ethanol pathway from *Thermoanaerobacterium saccharolyticum* improves ethanol production in *Clostridium thermocellum*. Metab Eng 42:175–184. https://doi.org/10.1016/j.ymben.2017.06.011.
24. Biswas R, Prabhu S, Lynd LR, Guss AM. 2014. Increase in ethanol yield via elimination of lactate production in an ethanol-tolerant mutant of *Clostridium thermocellum*. PLoS One 9:e86389–7. https://doi.org/10.1371/journal.pone.0086389.
25. Olson DG, Maloney M, Lanahan AA, Hon S, Hauser LJ, Lynd LR. 2015. Identifying promoters for gene expression in *Clostridium thermocellum*. Metab Eng Commun 2:23–29. https://doi.org/10.1016/j.meteno.2015.03.002.
26. Hon S, Lanahan AA, Tian L, Giannone RJ, Hettich RL, Olson DG, Lynd LR. 2016. Development of a plasmid-based expression system in *Clostridium thermocellum* and its use to screen heterologous expression of bifunctional alcohol dehydrogenases (*adhE*s). Metab Eng Commun 3:120–129. https://doi.org/10.1016/j.meteno.2016.04.001.
27. Espah Borujeni A, Salis HM. 2016. Translation initiation is controlled by RNA folding kinetics via a ribosome drafting mechanism. J Am Chem Soc 138:7016–7023. https://doi.org/10.1021/jacs.6b01453.
28. Chen J, Brevet A, Fromant M, Leveque F, Schmitter J-M, Blanquet S, Plateau P. 1990. Pyrophosphatase is essential for growth of *Escherichia coli*. J Bacteriol 172:5686–5689. https://doi.org/10.1128/jb.172.10.5686-5689.1990.
29. Wang Y, Zhang YHP. 2010. A highly active phosphoglucomutase from *Clostridium thermocellum*: cloning, purification, characterization and enhanced thermostability. J Appl Microbiol 108:39–46. https://doi.org/10.1111/j.1365-2672.2009.04396.x.
30. Bennett BD, Kimball EH, Gao M, Osterhout R, van Dien SJ, Rabinowitz JD. 2009. Absolute metabolite concentrations and implied enzyme active site occupancy in *Escherichia coli*. Nat Chem Biol 5:593–599. https://doi.org/10.1038/nchembio.186.
31. Williams JF, MacLeod JK. 2006. The metabolic significance of octulose phosphates in the photosynthetic carbon reduction cycle in spinach. Photosynth Res 90:125–148. https://doi.org/10.1007/s11120-006-9113-5.
32. Link H, Kochanowski K, Sauer U. 2013. Systematic identification of allosteric protein-metabolite interactions that control enzyme activity *in vivo*. Nat Biotechnol 31:357–361. https://doi.org/10.1038/nbt.2489.
33. Ding YHR, Ronimus RS, Morgan HW. 2000. Sequencing, cloning, and high-level expression of the *pfp* gene, encoding a PP_i-dependent phosphofructokinase from the extremely thermophilic eubacterium *Dictyoglomus thermophilum*. J Bacteriol 182:4661–4666. https://doi.org/10.1128/JB.182.16.4661-4666.2000.
34. Ding YR, Ronimus RS, Morgan HW. 2001. *Thermotoga maritima* phosphofructokinases: expression and characterization of two unique enzymes. J Bacteriol 183:791–794. https://doi.org/10.1128/JB.183.2.791-794.2001.
35. Reshetnikov AS, Rozova ON, Khmelenina VN, Mustakhimov II, Beschastny AP, Murrell JC, Trotsenko YA. 2008. Characterization of the pyrophosphate-dependent 6-phosphofructokinase from *Methylococcus capsulatus* Bath. FEMS Microbiol Lett 288:202–210. https://doi.org/10.1111/j.1574-6968.2008.01366.x.
36. Rozova ON, Khmelenina VN, Trotsenko YA. 2012. Characterization of recombinant PP_i-dependent 6-phosphofructokinases from *Methylosinus trichosporium* OB3b and *Methylobacterium nodulans* ORS 2060. Biochemistry (Mosc) 77:288–295. https://doi.org/10.1134/S0006297912030078.
37. Cui J, Stevenson D, Korosh T, Amador-Noguez D, Olson DG, Lynd LR. 2020. Developing a cell-free extract reaction (CFER) system in *Clostridium thermocellum* to identify metabolic limitations to ethanol production. Front Energy Res 8. https://www.frontiersin.org/articles/10.3389/fenrg.2020.00072/full.
38. Taillefer M, Rydzak T, Levin DB, Oresnik IJ, Sparling R. 2015. Reassessment of the transhydrogenase 'malate shunt' in *Clostridium thermocellum* ATCC 27405 through kinetic characterization of malic enzyme and malate dehydrogenase. Appl Environ Microbiol 81:2423–2432. https://doi.org/10.1128/AEM.03360-14.
39. Gibson DG. 2011. Enzymatic assembly of overlapping DNA fragments. Methods Enzymol 498:349–361. https://doi.org/10.1016/B978-0-12-385120-8.00015-2.
40. Olson DG, Lynd LR. 2012. Transformation of *Clostridium thermocellum* by electroporation. Methods Enzymol 510:317–330. https://doi.org/10.1016/B978-0-12-415931-0.00017-3.
41. Guss AM, Olson DG, Caiazza NC, Lynd LR. 2012. Dcm methylation is detrimental to plasmid transformation in *Clostridium thermocellum*. Biotechnol Biofuels 5:30. https://doi.org/10.1186/1754-6834-5-30.
42. Zhou J, Olson DG, Lanahan AA, Tian L, Murphy SJ-L, Lo J, Lynd LR. 2015. Physiological roles of pyruvate ferredoxin oxidoreductase and pyruvate formate-lyase in *Thermoanaerobacterium saccharolyticum* JW/SL-YS485. Biotechnol Biofuels 8:138. https://doi.org/10.1186/s13068-015-0304-1.
43. Sprenger GA, Schörken U, Sprenger G, Sahm H. 1995. Transaldolase B of *Escherichia coli* K-12: cloning of its gene, *talB*, and characterization of the enzyme from recombinant strains. J Bacteriol 177:5930–5936. https://doi.org/10.1128/jb.177.20.5930-5936.1995.
44. Olson DG, Hörl M, Fuhrer T, Cui J, Zhou J, Maloney MI, Amador-Noguez D, Tian L, Sauer U, Lynd LR. 2017. Glycolysis without pyruvate kinase in *Clostridium thermocellum*. Metab Eng 39:169–180. https://doi.org/10.1016/j.ymben.2016.11.011.
45. Clasquin MF, Melamud E, Rabinowitz JD. 2012. LC-MS data processing with MAVEN: a metabolomic analysis and visualization engine. Curr Protoc Bioinforma 37:14.11.1–14.11.23.
46. Melamud E, Vastag L, Rabinowitz JD. 2010. Metabolomic analysis and visualization engine for LC-MS data. Anal Chem 82:9818–9826. https://doi.org/10.1021/ac1021166.
47. Holwerda EK, Thorne PG, Olson DG, Amador-Noguez D, Engle NL, Tschaplinski TJ, van Dijken JP, Lynd LR. 2014. The exometabolome of *Clostridium thermocellum* reveals overflow metabolism at high cellulose

loading. Biotechnol Biofuels 7:155. https://doi.org/10.1186/s13068-014-0155-1.
48. Holwerda EK, Ellis LD, Lynd LR. 2013. Development and evaluation of methods to infer biosynthesis and substrate consumption in cultures of cellulolytic microorganisms. Biotechnol Bioeng 110:2380–2388. https://doi.org/10.1002/bit.24915.
49. Livak KJ, Schmittgen TD. 2001. Analysis of relative gene expression data using real-time quantitative PCR and the $2^{-\Delta\Delta CT}$ method. Methods 25:402–408. https://doi.org/10.1006/meth.2001.1262.
50. Walker C, Dien B, Giannone RJ, Slininger P, Thompson SR, Trinh CT. 2021. Exploring proteomes of robust *Yarrowia lipolytica* isolates cultivated in biomass hydrolysate reveals key processes impacting mixed sugar utilization, lipid accumulation, and degradation. mSystems 6:e00443-21. https://doi.org/10.1128/mSystems.00443-21.
51. Presley GN, Werner AZ, Katahira R, Garcia DC, Haugen SJ, Ramirez KJ, Giannone RJ, Beckham GT, Michener JK. 2021. Pathway discovery and engineering for cleavage of a β-1 lignin-derived biaryl compound. Metab Eng 65:1–10. https://doi.org/10.1016/j.ymben.2021.02.003.